FULL PAPER

Sub-ion-gyro scale magnetic field compressions generated by the solar wind interaction with the moon

Tomoko Nakagawa[1]*, Futoshi Takahashi[2], Yoshifumi Saito[3] and Hisayoshi Shimizu[4]

Abstract

Short-period magnetic enhancements were detected by the MAP-LMAG magnetometer onboard Kaguya orbiting the moon in the solar wind at an altitude of 100 km. The duration was typically 10 s, which corresponds to 0.5 degrees in latitude along the Kaguya orbit and a scale size of 15 km. The magnitude of the magnetic field was enhanced up to 1.5–3.6 times as large as that of the preceding quiet periods. No such magnetic enhancements were found in the upstream solar wind magnetic field. The short-period magnetic enhancements were categorized into 2 groups. One is the sub-ion-gyro-scale limb compression detected at the terminator region of the moon in a nearly constant solar wind magnetic field. The magnetic field flared away from the moon consistently with the previously known limb compressions. The scale size deduced from the duration was 11 km, 85 times as small as that of previously reported limb compressions. It is significantly smaller than the typical proton gyroradius 50–100 km in the solar wind at 1AU. The other types of magnetic enhancements appeared at crossings of magnetic discontinuities of the solar wind. Some of them were found on the nightside of the moon. A possible explanation is that they were magnetic fields compressed by the solar wind ions reflected at the moon channeled back along the current sheet of an interplanetary tangential discontinuity, similar to the hot flow anomalies observed at the Earth's bow shock. The reflected ions themselves were not detected on the nightside of the moon, while the magnetic field compressed by the expanding region can penetrate through the moon to be detected as magnetic field enhancements on the nightside of the moon.

Keywords Limb compression, Lunar external magnetic enhancement, Moon, Kaguya, Solar wind, Local crustal magnetic field, Magnetic anomaly, Hot flow anomalies, Diamagnetic cavity, Induced electric field
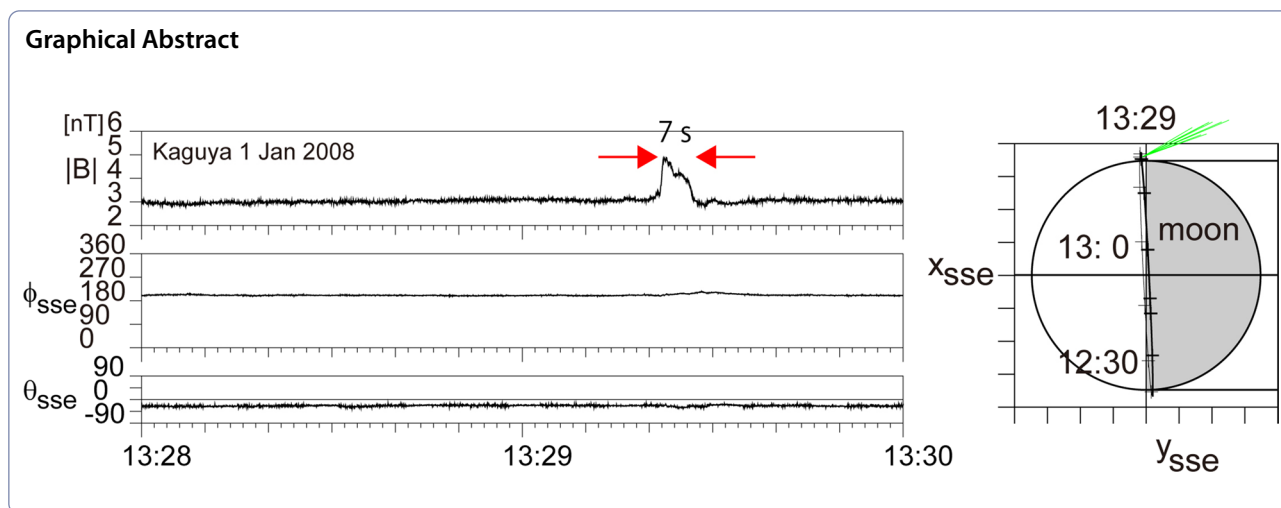
*Correspondence:
Tomoko Nakagawa
nakagawa@tohtech.ac.jp
Full list of author information is available at the end of the article

Nakagawa *et al. Earth, Planets and Space*   (2023) 75:60

Page 2 of 14

Graphical Abstract

Introduction

The solar wind interaction with the moon is governed by the absorption and reflection of solar wind particles by the lunar surface or the lunar crustal magnetic field. The absence of a global dipole field enables direct access of the solar wind to the lunar surface. Most solar wind particles are absorbed by the lunar surface, creating the lunar wake downstream of the moon (Lyon et al. 1967; Schubert and Lichtenstein 1974; Ogilvie et al. 1996; Bosqued et al. 1996), while a small fraction of solar wind particles is backscattered by the lunar surface in the form of plasmas or energetic neutral atoms or reflected by the local crustal magnetic field (Saito et al. 2008, 2010, 2012; Wang et al. 2010; Lue et al. 2011; Futaana et al. 2001; McComas et al. 2009; Wieser et al. 2009, 2011; Poppe et al. 2014, 2017).

Magnetic perturbations generated by the solar wind interaction with the moon have attracted great attention since the early stage of exploration of the moon. Although the solar wind magnetic field passing through the moon is essentially unimpeded due to the low electric conductivity of the moon (Sonett 1982; Lin et al. 1998), slight enhancements in the magnitude of the magnetic field were found in the wake, together with magnetic field perturbations at the wake boundary (Colburn et al. 1967; Ness et al. 1968; Russell and Lichtenstein 1975; Owen et al. 1996; Fatemi et al. 2013; Holmström et al. 2012). The reflected or backscattered solar wind particles decelerate the bulk flow and modify the velocity distribution function of the solar wind plasma to cause various kinds of wave activities (Halekas et al. 2006b; Nakagawa et al. 2011, 2012; Tsugawa et al. 2011, 2012; Harada et al. 2015; Harada and Halekas 2016; Nakagawa 2016). Above the intense local lunar crustal magnetic field termed magnetic anomalies, where solar wind reflection is efficient, the deceleration of the solar wind flow causes magnetic compression, which propagates at the speed of magnetohydrodynamic (MHD) waves. When the magnetic anomaly comes across the terminator, the wavefront flares away from the moon and can be detected as a limb shock or a limb compression if it reaches a spacecraft (Russell and Lichtenstein 1975; Lin et al. 1998; Halekas et al. 2017). Above the dayside anomaly, magnetic perturbations can be detected as lunar external magnetic enhancements (Halekas et al. 2006a). A large-scale limb shock arising from a major magnetic anomaly was detected by Lunar Prospector at an altitude of 100 km from the lunar surface (Lin et al. 1998). It lasted for 10 min and was detected recurrently in successive revolutions of the Lunar Prospector when the spacecraft came across the magnetic anomaly until the solar wind dynamic pressure increased and overwhelmed the surface fields.

On the other hand, major magnetic anomalies are not the only drivers of limb compression. ARTEMIS detected a limb shock with a duration of a few minutes, which was supposed to be generated by a small-scale crustal field via reflected protons (Halekas et al. 2014).

The scale of the crustal magnetic field ranges from a few thousand kms down to less than 1 km (Dyal et al. 1974; Hood et al. 2001; Mitchell et al. 2008; Tsunakawa et al. 2015). It is expected that small-scale crustal fields also interact with the solar wind, but observational studies have been difficult because small-scale events are often masked by large-scale phenomena. Zimmerman et al. (2015) carried out kinetic simulations of solar wind interaction with a small-scale crustal magnetic field and showed that a shallowly buried dipole

Nakagawa *et al. Earth, Planets and Space*   (2023) 75:60

Page 3 of 14

magnetization can produce a mini-magnetosphere smaller than 1 km.

This paper focuses on short-period (< 10 s) magnetic enhancements generated via solar wind interaction with the moon and detected by Kaguya on its orbit at an altitude of 100 km from the lunar surface. They are thought to be sub-ion-gyro-scale limb compressions whose scale size was on the order of 10 km or a magnetic compression generated by reflected protons channeled back along interplanetary tangential discontinuities. The spatial extent on the order of 10 km along the Kaguya orbit estimated from their duration is much smaller than the typical proton gyroradius at the Kaguya position, suggesting that they are not in the magnetohydrodynamic scale but in kinetic scale in which separation of motion of ions and electrons would be important, as seen in the formation of an ambipolar electric field.

Data

The magnetic field data used in this study were obtained by the Lunar Magnetometer (LMAG) subsystem of the Magnetic field and Plasma experiment (MAP) onboard the Kaguya spacecraft (Kato et al. 2010) during the period from January 1, 2008 to December 31, 2008. The spacecraft was on its polar orbit encircling the moon at an altitude of 100 km within 118 min. MAP-LMAG obtained magnetic field vectors with a sampling frequency of 32 Hz (Shimizu et al. 2008; Takahashi et al. 2009; Tsunakawa et al. 2010).

The plasma density and velocity were calculated from the velocity distribution function obtained by the Kaguya Plasma energy Angle and Composition Experiment (MAP-PACE) instrument (Saito et al. 2010). Ion density and bulk velocity were obtained separately from 2 sensors, the Ion Mass Analyzer (IMA) sensor facing the moon and the Ion Energy Analyzer (IEA) looking nadir direction, and then combined to produce total ion density and bulk velocity.

Unperturbed solar wind magnetic field and plasma conditions were monitored using Level 2 data from Magnetic Field experiment (MAG) and Solar Wind Electron Proton Alpha Monitor (SWEPAM) onboard Advanced Composition Explorer (ACE) spacecraft. The data were extracted from the ACE Science Center (http://www.srl.caltech.edu/ACE/ASC/index.html). OMNIWeb Plus data were used in cases where ACE Level 2 data were not available.

Results

A sub-ion-gyro-scale limb compression on January 1, 2008
Figure 1 shows a short-period magnetic enhancement found in a two-hour summary plot of the 1 s averaged magnetic field observed by Kaguya on 1 January 2008. The black curves in panels (a)–(c) are the magnetic field observed by Kaguya at an altitude of 100 km above the lunar surface, while the gray curves are the solar wind magnetic field observed by ACE far upstream of the moon, shifted by 1.06 h for the solar wind with a speed of 365 km s^{-1} to travel the distance from ACE to Kaguya.
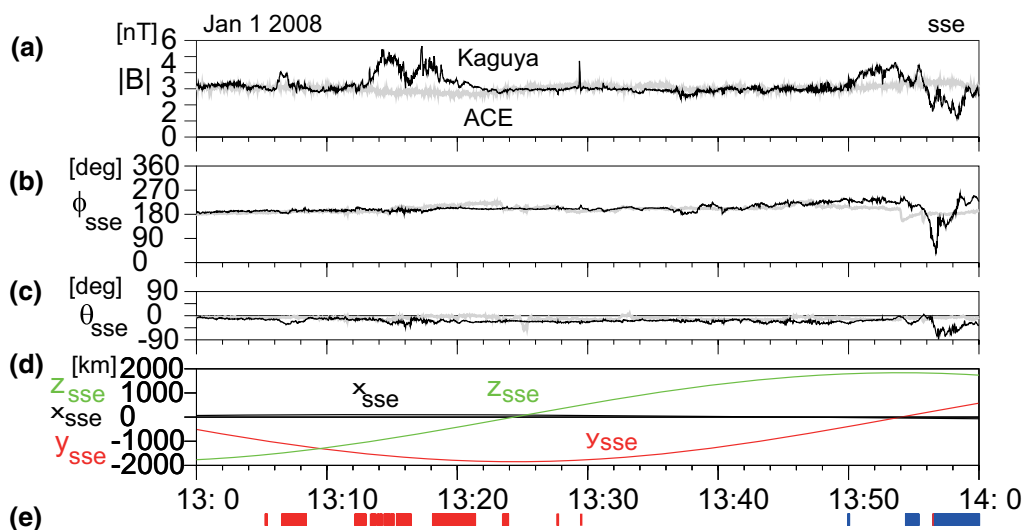
Fig.1 A short-period magnetic enhancement detected by Kaguya at 100 km above the moon. **a** The magnitude, **b** the azimuthal angle, and **c** the latitude angle of the magnetic field observed by Kaguya (black curves) in the Selenocentric Solar Ecliptic (SSE) coordinate system compared with that of the upstream solar wind observed by ACE (gray curve) in the Geocentric Solar Ecliptic (GSE) system shifted by a travel time of 1.06 h from ACE to Kaguya. **d** The position of Kaguya in SSE coordinates. **e** The magnetic connection between Kaguya and the dayside (red) or nightside (blue) lunar surface estimated from linear extrapolation of the magnetic field

Nakagawa *et al. Earth, Planets and Space* (2023) 75:60

Page 4 of 14

At 13:29, a spike-like, short-period enhancement is recognized in the magnitude of the magnetic field observed by Kaguya (Fig. 1a). The magnetic enhancement was not seen in the upstream solar wind magnetic field observed by ACE.

The magnetic enhancement was not accompanied by variation in the direction of the magnetic field in Fig. 1b, c. Accordingly, the change in the magnetic field vector was parallel to the magnetic field vector itself. The vector normal to the compression surface must be perpendicular to the variation vector and thus the magnetic field, and the wave surface should be parallel to the magnetic field.

Figure 2 shows the position of the spacecraft in (a) Geocentric Solar Ecliptic (GSE) coordinates and in (b)–(d) Selenocentric Solar Ecliptic (SSE) coordinates at the time of detection of the magnetic enhancement. The moon was in the solar wind upstream of the Earth's bow shock. Kaguya was above the dawnside terminator, a favorable position for the detection of limb compression. Green bars in panels (b)–(d) represent 1-s averaged magnetic field vectors plotted on the orbit of Kaguya during the period from 13:29:20 to 13:29:27. The magnetic field flared away from the lunar surface with a flaring angle of 16°. The magnetic compression with the wave surface flaring away from the moon above the limb is a signature of limb compression. For this event, the intrinsic solar

wind magnetic field was in the same direction as the flaring magnetic field.

Figure 3a shows an enlarged view of the magnetic field enhancement obtained at a sampling frequency of 32 Hz. Until 13:29:20, the magnetic field was stable, and the magnitude was 3.0 nT. It began to increase slowly at 13:29:20, jumped up to its maximum of 4.9 nT abruptly at 13:29:22, and then decreased in two steps at 13:29:24 and 13:29:26. The magnitude returned to the initial value at 13:29:27. The duration of the enhancement was as short as 7.0 s. Multiplied by the velocity of the orbital motion of Kaguya, the 7 s duration corresponds to 0.36° in latitude, or 11 km along the polar orbit. It is 85 times smaller than the limb shock reported by Lin et al. (1998). It was much smaller than the ion inertia length of 180 km calculated from the Alfvén speed 52 km s^{-1} and the proton gyrofrequency 0.29 rad/s.
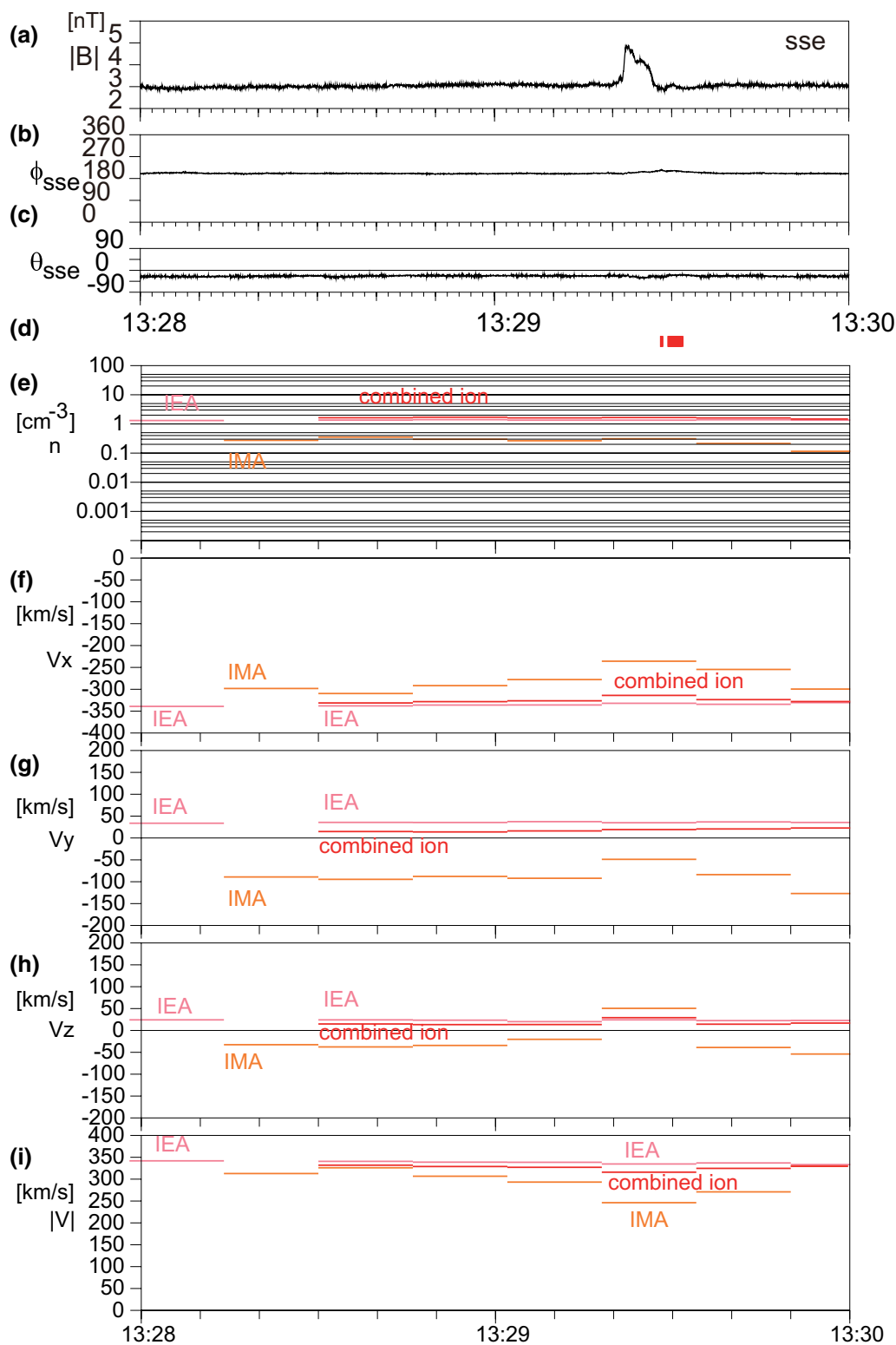
Figure 3e–i shows the ion density and velocity observed by MAP-PACE onboard Kaguya. The plasma number density 1.6×10^6 m^{-3} and the bulk velocity on the order of 330 km s^{-1} (red lines) were smaller than those of a typical solar wind. In such a slow solar wind, magnetic perturbations originating from the lunar surface can travel a significant distance before they are convected down by the bulk flow of the solar wind and can be detected by a spacecraft at an altitude 100 km from the lunar surface especially at the limb of the moon (Halekas et al. 2006a).
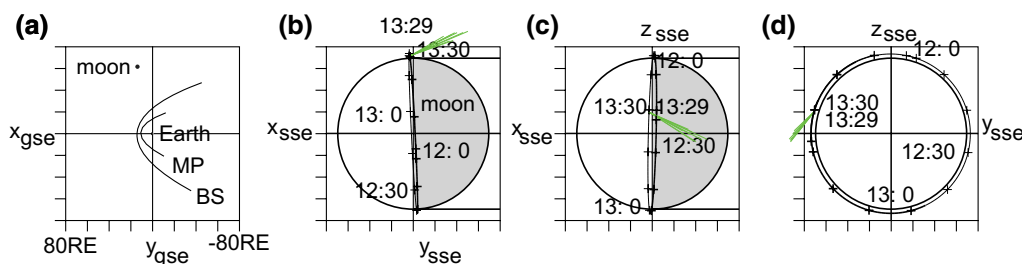
Fig. 2 Kaguya position and magnetic field vectors of limb compression on 1 January 2008. **a** Position of the moon in the GSE coordinate system, with the nominal bow shock (BS) and magnetopause (MP) of the Earth, and (**b**–**d**) Position of Kaguya in the SSE coordinate system, projected onto the (**b**) x–y, **c** x–z and (**d**) y–z planes. Thin-lined curves show that Kaguya was behind the moon. Green bars represent 1-s averaged magnetic field vectors observed by Kaguya during the period from 13:29:20 to 13:29:27

(See figure on next page.)
Fig. 3 High-time resolution magnetic field and ion momenta of short-period magnetic enhancement on 1 January 2008. **a** The magnitude, **b** the azimuthal angle and **c** the inclination of the magnetic field observed by MAP-LMAG at a sampling frequency of 32 Hz during the period from 13:28 to 13:30 on 1 January 2008. The magnetic field enhancement is significant from 13:29:20 to 13:29:27 with no directional change. **d** Magnetic connection between Kaguya and the lunar surface estimated from linear extrapolation of the magnetic field line at Kaguya. The magnetic field line at Kaguya did not connect to the lunar surface during the magnetic field enhancement. **e** Ion densities observed by IEA (pink) and IMA (orange) sensors of MAP-PACE onboard Kaguya, looking zenith and nadir directions, respectively, combined to obtain the total ion density (red). **f** x_{SSE}, **g** y_{SSE}, **h** z_{SSE} components of the ion velocity in SSE coordinates and (**i**) the ion bulk speed |V|. During the magnetic enhancement in **a**, only the ion component from the nadir direction (orange) fluctuated

**Fig. 3** (See legend on previous page.)

Nakagawa *et al. Earth, Planets and Space*   (2023) 75:60

Page 6 of 14

From these characteristics, the short-period magnetic enhancement is interpreted as limb compression.

The limb compression was accompanied by a slight deceleration of the ion bulk velocity. Figure 3f, i shows a slight deceleration of ions during a 16 s period from 13:29:18.386 to 13:29:34.386 which included the limb compression. Deceleration is clearer in the data from the IMA sensor (the orange lines in Fig. 3f–i), which detects ions coming from the moon. This suggests that ion reflection by the moon was intensified during limb compression. Figure 4 shows the energy-time spectra of the plasma particles during an 8 min period from 13:24 to 13:32. The intensification of the reflected ions was observed by the IMA sensor at 13:29 (Fig. 4d) simultaneously with the short-period enhancement of magnitude of the magnetic field (Fig. 4e).

We can estimate the propagation speed of the magnetic compression from the flaring angle 16°, which is determined by the ratio of the propagation speed of magnetic compression and the solar wind convection speed. Here, the solar wind speed was 330 km s^{-1}, and the wave speed was estimated to be approximately 91 km s^{-1}. It is consistent with the speed of the fast mode wave if we assume the ion sound speed to be approximately 75 km s^{-1}, as the Alfvén speed was 52 km s^{-1} calculated from the ion number density 1.6×10^6 m^{-3} and the magnitude of the
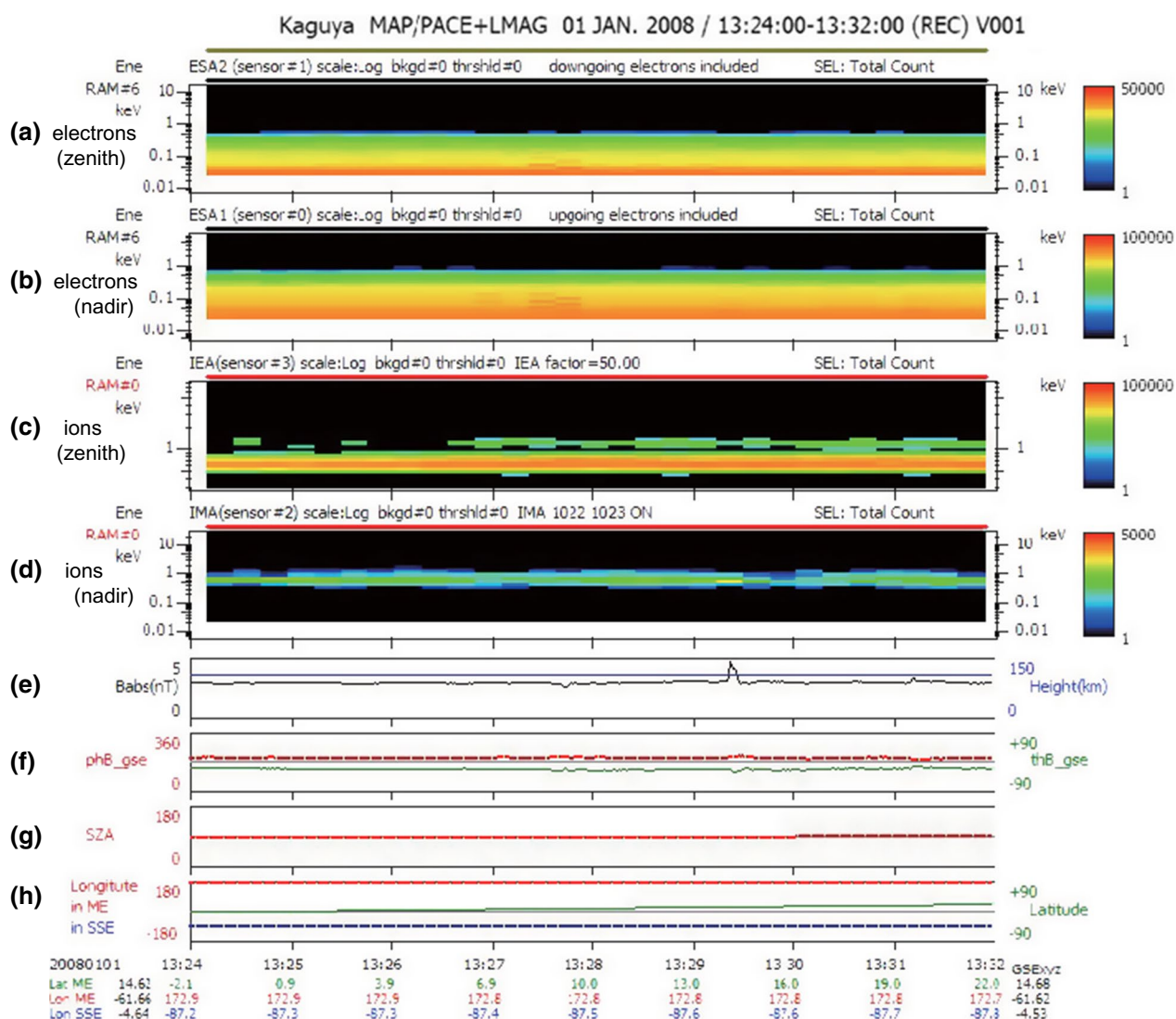
Fig. 4 Energy time spectra of plasma particles obtained by MAP/PACE onboard Kaguya on January 1, 2008. **a** Electrons detected by ESA2 sensor (on zenith-looking panel), **b** electrons detected by ESA1 sensor (on nadir-looking panel), **c** ions detected by IEA sensor (on zenith-looking panel), **d** ions detected by IMA sensor (on nadir-looking panel), **e** magnitude and **f** directions of magnetic field measured by LMAG, **g** solar zenith angle of Kaguya, and **h** longitude and the latitude of Kaguya in SSE and ME coordinate systems

Nakagawa *et al. Earth, Planets and Space*   (2023) 75:60

Page 7 of 14

ambient magnetic field 3.0 nT. Using the sound speed 75 km s^{-1} thus obtained we can estimate the proton gyroradius of the order of 260 km. The scale size of the limb compression was one order smaller than the proton gyroradius.

An attempt was made to find a local crustal magnetic field structure that drove the limb compression. Figure 5a, b illustrates a 3-dimensional view of Kaguya (represented by a yellow cube) at 13:29. The lunar surface is color-coded with the magnitude of the Lunar Surface Vector Mapping of the Kaguya LMAG (Tsunakawa et al. 2015). The magnetic field line at Kaguya (a purple line extending from the cube) did not connect the spacecraft and the lunar surface (Fig. 5b). The closest distance of the line of force of the magnetic field linearly extrapolated from Kaguya was 68 km from the lunar surface. An open square in Fig. 5c marks the closest point. The magnitude of the surface magnetic field below the closest point was smaller than 12 nT. There was a stronger magnetic anomaly on the east (solar side) of Kaguya (southwest of the closest point). It should be noted that the actual line of force of the magnetic field is not straight and that the crustal magnetic field could be highly deformed under the condition of shallow incidence angle of the solar wind flow near the limb (Deca et al. 2021).

The limb compression was not detected recurrently in the next revolution of Kaguya, although the solar wind plasma and magnetic field conditions remained nearly the same.

Hot flow anomaly on August 5, 2008
Figure 6 shows another short-period magnetic enhancement observed by Kaguya on August 5, 2008. The black curves on the top 4 panels show the magnetic field observed by Kaguya, and the gray curves are the magnetic field observed by ACE approximately 1.2167×10^4 km upstream in the solar wind shifted by the travel time 62.4 min calculated with the solar wind speed 325 km s^{-1}. At 3:28:35, Kaguya detected a jump in the magnitude of the magnetic field from 0.89 nT to 3.36 nT, 3.8 times as large as the initial value, followed by another jump down to 1.28 nT. No such spiky magnetic enhancement was found in the upstream solar wind. Instead, there was a magnetic discontinuity at the shifted time of

3:29 (in reality, 2:27 at the ACE position), where the magnitude |B| of the magnetic field jumped from 3 to 1 nT. The large jump in a magnetic field with no variation in the solar wind velocity (gray dots in Fig. 6g–j) suggests that it was a tangential discontinuity (e.g., Neugebauer et al. 1984). The discontinuity was also recognized in the Kaguya magnetogram at 3:28 (Fig. 6a–d).

Figure 7 shows the position of Kaguya at the time of magnetic enhancement detection. It cannot be a limb compression because it was detected on the nightside of the moon. Red bars indicate the vectors of the enhanced magnetic field embedded in the ambient magnetic field (green bars).

Figure 8 shows an expanded magnetogram obtained at a sampling frequency of 32 Hz. The magnitude |B| of the magnetic field began to increase at 3:28:35.3, peaked at 3:28:41.7, and returned to the initial level at 3:28:44.6. The duration of the enhancement was as short as 9.3 s. Here, the start and end times were defined as moments at which the magnitude |B| of the magnetic field exceeded 5 min averages of |B| of pre- and post-event, respectively.

Discussion
Scale size of the limb compression on January 1, 2008
The 7 s duration of the magnetic enhancement detected on January 1, 2008 corresponds to 0.36° in latitude, or 11 km along the polar orbit. It is smaller than the longitudinal shift of approximately 1° of Kaguya orbit per 1 revolution, which corresponds to 29 km at Kaguya latitude 14.1° at the detection of this limb compression. This may account for the nonrecurrent detection of compression.

The spatial extent 0.36° is close to the spatial resolution of 0.2° of the Lunar Surface Vector Mapping of Kaguya LMAG (Tsunakawa et al. 2015). The driver magnetic structure of the limb compression may not be resolved in the Lunar Surface Vector Mapping of the Kaguya LMAG. On the basis of kinetic simulations, Zimmerman et al. (2015) showed that a km-scale strong magnetic field at the terminator region of the moon changes the motion of solar wind ions and electrons, creating an ambipolar electric field and a mini-magnetosphere that can reflect solar wind ions. A small-scale crustal magnetic field that cannot be resolved in the Lunar Surface Vector Mapping of Kaguya LMAG might have created a mini-magnetosphere at dawn to reflect the solar wind protons, causing

(See figure on next page.)

Fig. 5 Kaguya position at 13:29 on January 1, 2008, and the lunar crustal magnetic field. Kaguya is represented by a yellow cube (not in scale). The line of force of the magnetic field observed at Kaguya is represented by a purple bar extending from Kaguya. The orange line points to the Sun. The red, green, and blue lines indicate the x_{ME}, y_{ME}, and z_{ME} axes, respectively, of the mean Earth/Polar Axis (ME) reference system, where the x_{ME} axis is defined by the mean Earth direction, and the z_{ME} axis is defined by the mean rotational pole (LRO Project et al. 2008). The lunar surface is color-coded with the magnitude of the lunar crustal field at 0 km altitude (Tsunakawa et al. 2015). **a** A dawnside view. **b** A view from dayside, southern hemisphere. **c** An enlarged projection of Kaguya (a cross) and the closest approach of the linearly extrapolated line of force of the magnetic field at Kaguya (a square) radially onto the lunar surface
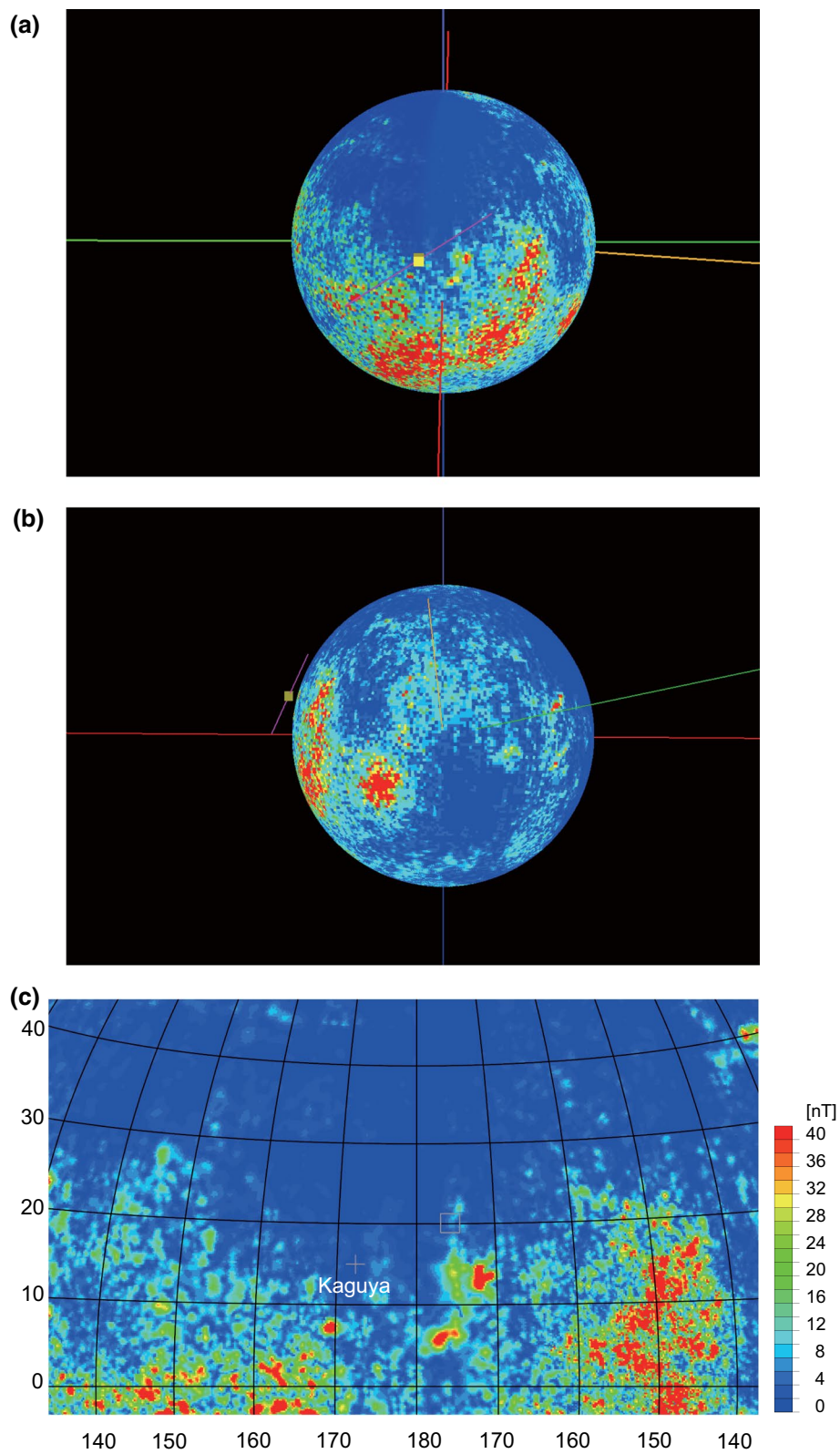
**Fig. 5** (See legend on previous page.)
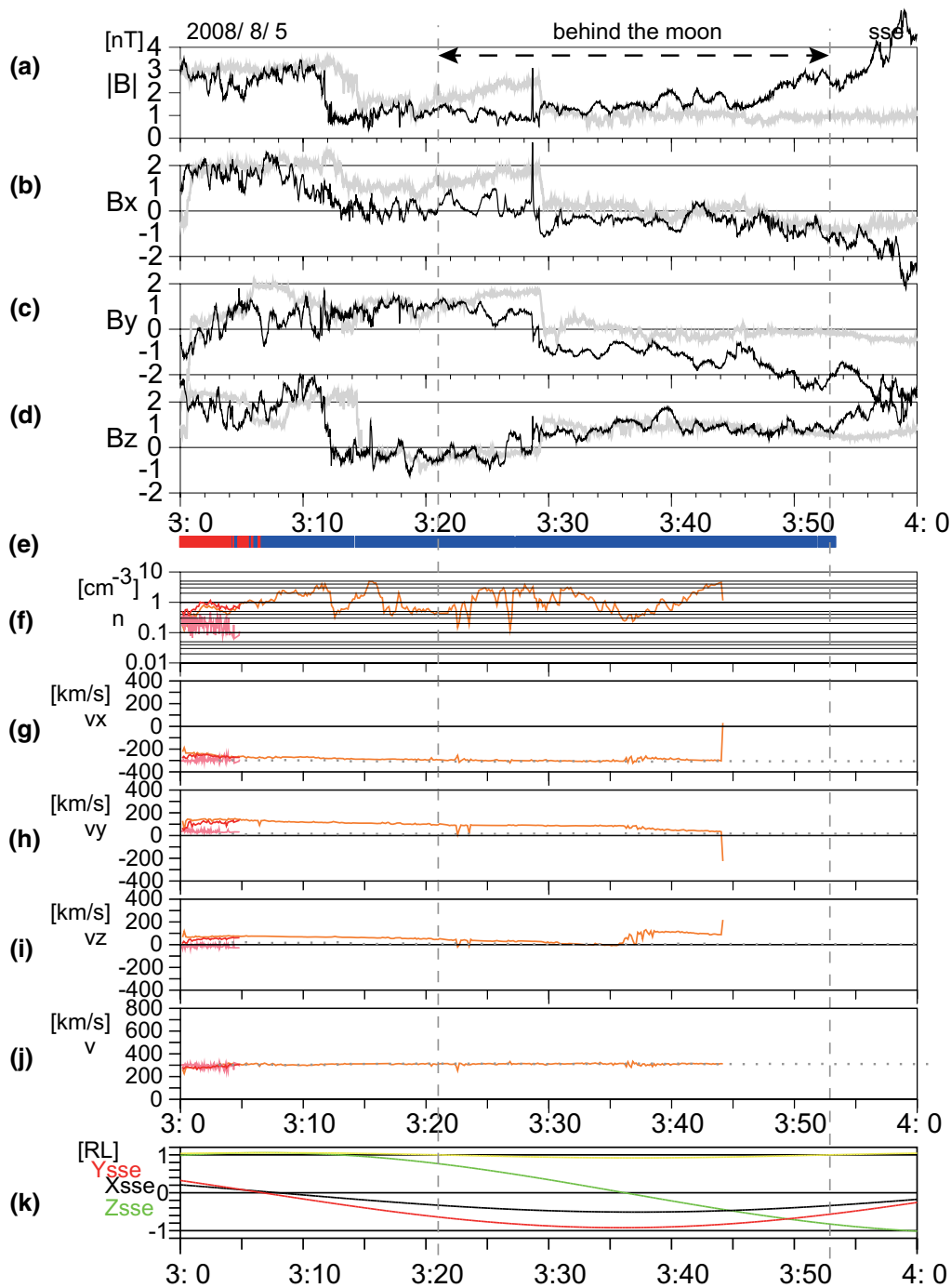
Fig. 6 Magnetic compression at a hot flow anomaly on August 5, 2008. **a–d** The magnetic field observed by Kaguya (black curves) in SSE coordinates and by ACE (gray curve) in the GSE coordinate system shifted by a travel time of 1.04 h from ACE to Kaguya. **e** Magnetic connection between Kaguya and the dayside (red) or nightside (blue) surface of the moon. **f** Ion density and **g–j** bulk velocity observed by MAP/PCE. Pink, orange and red curves are measurements from IEA, IMA sensors and their combination. Gray dots are upstream solar wind parameters observed by ACE. **k** The position of Kaguya in SSE coordinates. The yellow line shows $\sqrt{y_{SSE}^2 + z_{SSE}^2}$ normalized by the lunar radius. Vertical dashed lines mark Kaguya crossings of the boundary of the shadow of the moon

Nakagawa *et al. Earth, Planets and Space*   (2023) 75:60

Page 10 of 14
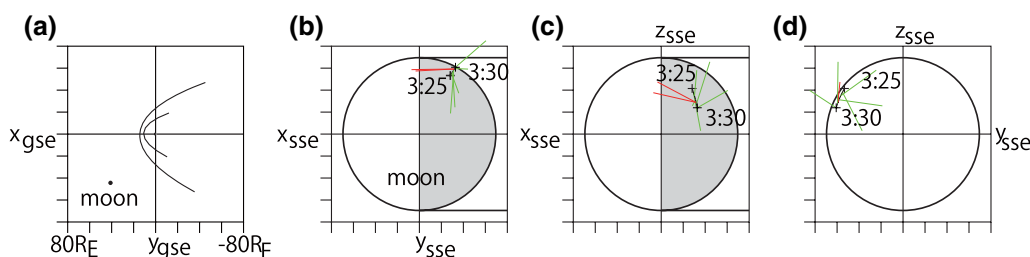
Fig. 7 Kaguya position and magnetic field vectors produced by a hot flow anomaly on 5 August 2008. The format is the same as in Fig. 2. Red bars represent directions of the 1-s averaged magnetic field vectors of the short-period magnetic enhancement at approximately its maximum intensity at 3:28:41, while green bars represent ambient magnetic field vectors plotted every 60 s during the period from 3:25 to 3:30
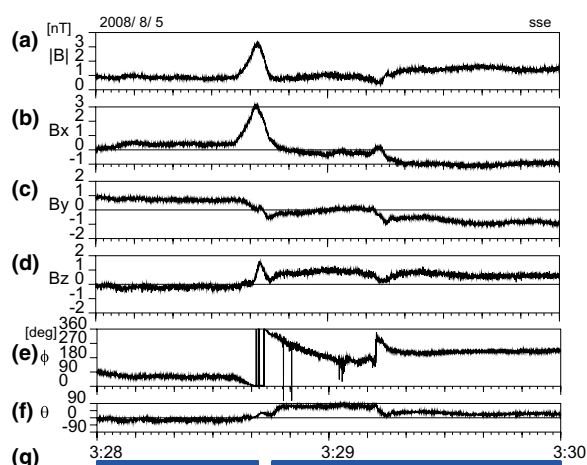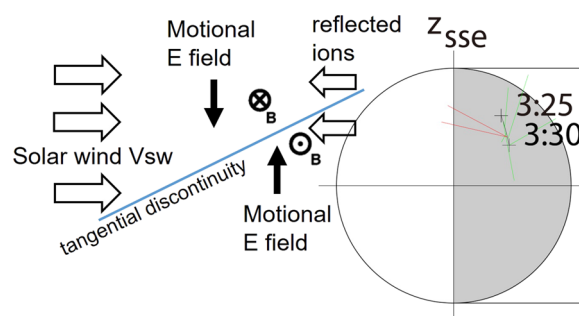

Fig. 8 High time resolution magnetic field of a hot flow anomaly on August 5, 2008. **a**–**d** The magnitude and the x_{SSE}, y_{SSE}, z_{SSE} components of the magnetic field in SSE coordinates, **e** the azimuth and **f** the latitude angles observed by Kaguya at a sampling rate of 32 Hz. **g** Magnetic connection between Kaguya and the nightside surface of the moon


Fig. 9 A schematic illustration of hot flow anomaly formation on August 5, 2008. The motional electric fields induced by the reflected ions point toward the tangential discontinuity on both sides of the discontinuity surface

a reduction in the solar wind bulk speed and compression of the magnetic field.

There is another possibility that the reflected ions were originating from an intense crustal field far from the closest point of the magnetic field or detection site of the compression. It should be noted that the proton reflection is not specular nor uniform, but highly variable depending on the topology of the crustal field and the solar wind conditions, as discussed by Deca and Divin (2017).

Possible hot flow anomaly on August 5, 2008

In Fig. 6, we have seen a magnetic enhancement at an interplanetary tangential discontinuity. It is a common signature with hot flow anomalies at the Earth's bow shock. A hot flow anomaly, also termed a hot diamagnetic cavity, is formed by solar wind ions reflected by the Earth's bow shock interacting with an interplanetary

tangential discontinuity (Schwartz et al. 1995, 2000). The reflected ions are channeled back along the current sheet of the discontinuity under the condition that their motional electric field points toward the current sheet on at least one side of the discontinuity, resulting in a hot ion population of deflected solar wind flow that expands, compressing the magnetic field at the edge and producing magnetic enhancements (Burgess 1989; Thomas et al. 1991; Schwartz et al. 2000; Eastwood et al. 2008). There is a possibility that the same mechanism worked at the moon. The solar wind ions reflected by the moon or the lunar crustal magnetic field would be accelerated toward the discontinuity surface if the motional electric field points toward the current sheet. If we assume the sunward motion of reflected ions, they would cross the upstream magnetic fields $\mathbf{B}_{up} = (0.08, 0.75, 0.23)$ nT (a 2 min average from 3:26:30 to 3:28:30) and induce a northward-directed electric field, while in the downstream magnetic field $\mathbf{B}_{down} = (-0.65, -0.94, 0.66)$ nT (a 2 min average for 3:29:30–3:31:30), the ions induce a southward-directed electric field. Here, we assume the downstream region as a period of a stable magnetic field after 3:29:30 because there was another magnetic perturbation at 3:29:12 in Fig. 8, which bound a transition

Nakagawa *et al. Earth, Planets and Space*   (2023) 75:60

Page 11 of 14

Table 1 Short period magnetic enhancements detected by Kaguya

#	yr/mm/dd	hh:mm:ss	Duration [s]	|B| max [nT]	|B| pre [nT]	Kaguya Altitude [km]	Solar wind V_x [km s^{-1}]	Solar wind density [× 10^6 m^{-3}]	Dynamic pressure* [nPa]	IP magnetic discontinuity
1	2008/1/1	13:29:20.0442	6.969	4.9	3.0	108	Kaguya 330 ACE 380	Kaguya 1.6 ACE -	0.29 -	no
2	2008/3/10	09:26:45.0810	2.250	6.6	4.5	91	Kaguya -i ACE 630 WIND 652	Kaguya -i ACE - WIND 2.4	- - 1.7	no
3	2008/6/8	05:43:06.0615	9.969	8.5	3.7	92	Kaguya -i ACE 501	Kaguya -i ACE 3.6	- 1.5	yes
4	2008/8/5	03:28:35.3177	9.281	3.4	0.9	90	Kaguya -n ACE 310 WIND 315	Kaguya -n ACE - WIND 9.0	- - 1.5	yes
5	2008/11/27	04:26:28.0460	3.469	6.0	3.3	110	Kaguya - ACE 600	Kaguya - ACE 2	- 1.2	yes
6	2008/12/21	23:50:28.0383	9.969	5.8	3.6	101	Kaguya -n ACE 300 WIND 296	Kaguya -n ACE - WIND 5.7	- - 0.83	yes

(-) no data (-n) nightside (-i) Kaguya IMA no data (*) typical value of dynamic pressure was 1.7 nPa calculated from the solar wind speed 450 km s^{-1} and density 5 × 10^6 m^{-3}
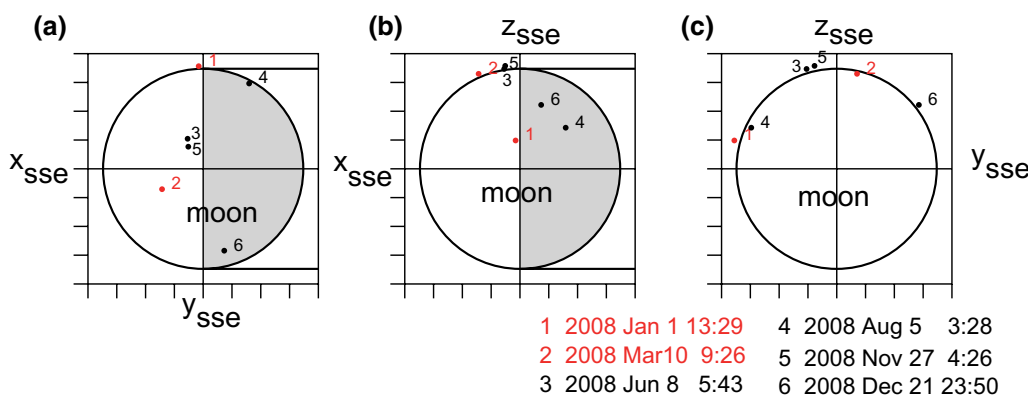
Fig. 10 Distribution of short-period magnetic enhancements detected by Kaguya. Position of Kaguya at the detection of short-period magnetic enhancements projected on the **a** $x − y$, $x − z$, and $y − z$ planes of the SSE coordinate system. Red dots (#1 and #2) are limb compressions found in the constant solar wind magnetic field, and black dots are those found at interplanetary magnetic discontinuities. Event numbers are the same as those in Table 1

region from 3:28:35 to 3:29:12 in which the azimuthal angle ϕ of the magnetic field turned from 60 to 210°. The induced electric fields point toward the discontinuity surface, as illustrated schematically in Fig. 9, which is favorable for hot flow anomaly conditions. The vector normal to a discontinuity surface (0.84, − 0.24, 0.49) was calculated with the vector product $\mathbf{B}_{up} \times \mathbf{B}_{down}$ for a tangential discontinuity. The minimum variance analysis (Sonnerup and Cahill 1967) was not employed because the magnetic field variation during the transition must be perturbed by the hot flow anomaly.

The ions accelerated toward the current sheet of the tangential discontinuity are expected to form a high-pressure region to compress the ambient magnetic field. The reflected ions themselves cannot be detected by Kaguya behind the moon, but it is expected that the compressed magnetic field can penetrate through the moon due to the low conductivity of the moon.

Search for hot plasma to compress the magnetic field
We assumed that the magnetic compression detected on August 5, 2008, was produced by hot plasmas channeled back along the tangential discontinuity, but we cannot examine the presence of hot plasmas themselves because the spacecraft was on the other side of the moon. An attempt was made to find similar magnetic compressions on the dayside of the moon, where the reflected plasmas can be detected. Table 1 shows a list of the 6 smallest scale magnetic field compressions detected by visual inspection of the magnetograms obtained by Kaguya following the criteria:

1) Magnetic enhancement $\Delta|B| > 1.9$ nT in a short period < 10 s

2) Preceded by a magnetically quiet period (not embedded in larger magnetic enhancements).

Four events (#3−#6) are candidates of hot flow anomalies found at interplanetary magnetic discontinuities, while the others are limb compressions found in a constant solar wind magnetic field. Figure 10 shows the distribution of the 6 events in SSE coordinates. All the events were found in the northern hemisphere, perhaps because such small-scale events cannot be detected if they were embedded in larger-scale magnetic perturbations or large-amplitude wave activities produced by solar wind reflection by the major magnetic anomalies in the southern hemisphere. It suggests that small-scale magnetic enhancements occur more often than detected. Red dots (events #1 and #2) are candidate limb compressions. They were found above the terminator. Black dots indicate magnetic enhancement found at interplanetary magnetic discontinuities. Events #4 and #6 are thought to be produced by hot flow anomalies because they were found downstream of the moon and thus cannot be limb compressions. Events #3 and #5 are candidate hot flow anomalies detected on the dayside terminator region, although there is a possibility that they were limb compressions. Unfortunately, the plasma measurement was not available during the moments of the two dayside events.

Conclusions
Short-period magnetic enhancements with durations less than 10 s were detected by Kaguya 100 km above the moon. They are thought to be generated through solar wind interaction with the moon. Two events out of 6 examples were found in the unperturbed solar

Nakagawa *et al. Earth, Planets and Space*   (2023) 75:60

Page 13 of 14

wind and thought to be sub-ion-gyro-scale limb compressions whose scale was on the order of 11 km, smaller than the ion inertia length and the proton gyro radius. Other short-period magnetic enhancements were found at interplanetary tangential discontinuities. Two of them found on the nightside of the moon are thought to be generated on the dayside by magnetic field compression by the reflected solar wind ions channeled back along the current sheet of interplanetary tangential discontinuities, similar to hot flow anomalies at the Earth's bow shock, and then penetrated through the moon, but no hot plasmas that would evidence this scenario have yet been detected. Such small-scale magnetic structures are thought to be present more frequently than detected but are not noticed because they are embedded in larger magnetic perturbations or wave activities.

Author contributions
TN performed the data analysis and manuscript preparation. FT was involved in the magnetic field observation by Kaguya/MAP-LMAG and contributed to the analysis of the LMAG data. YS was responsible for the plasma measurements by the Kaguya/MAP-PACE instrument. HS contributed to calibrating the lunar magnetometer LMAG. All authors contributed to the discussion and conclusions of this study. All authors read and approved the final manuscript.

Availability of data and materials
The Kaguya MAP-LMAG and MAP-PACE data are available at the Kaguya (SELENE) Data Archive (http://l2db.selene.darts.isas.jaxa.jp/index.html.en). ACE level 2 data are available at the ACE Science Center (ASC) (http://www.srl.caltech.edu/ACE/ASC/level2/). OMNIWeb Plus data are available at https://omniweb.gsfc.nasa.gov/.

Declarations

Ethics approval and consent to participate
Not applicable.

Consent for publication
Not applicable.

Competing interests
The authors declare that they have no competing interests.

Author details
[1]Department of Information and Communication Engineering, Tohoku Institute of Technology, 35-1 Yagiyama Kasumi-cho, Taihaku-ku, Sendai 982-8577, Japan. [2]Department of Earth and Planetary Sciences, Faculty of Science, Kyushu University, 744 Moto-oka, Nishi-ku, Fukuoka 819-0395, Japan. [3]Institute of Space and Astronautical Science, Japan Aerospace Exploration Agency, Yoshinodai 1-chome, Sagamihara 252-5210, Japan. [4]Earthquake Research Institute, University of Tokyo, 1-1-1, Yayoi, Bunkyo-ku, Tokyo 113-0032, Japan.

References

Bosqued JM, Lormant N, Rème H, d'Uston C, Lin RP, Anderson KA, Carlson CW, Ergun RE, Larson D, McFadden J, McCarthy MP, Parks GK, Sanderson TR, Wenzel K-P (1996) Moon-solar wind interaction: first results from the WIND/3DP experiment. Geophys Res Lett 23:1259–1262. https://doi.org/10.1029/96GL0030

Burgess D (1989) On the effect of a tangential discontinuity on ions specularly reflected at an oblique shock. J Geophys Res 94(A1):472–478. https://doi.org/10.1029/JA094iA01p00472

Colburn DS, Currie RG, Mihalov JD, Sonett CP (1967) Diamagnetic solar-wind cavity discovered behind moon. Science 158(3804):1040–1042

Deca J, Divin A (2017) Reflected charged particle populations around dipolar lunar magnetic anomalies. Astrophys J 829:60. https://doi.org/10.3847/0004-637X/829/2/60

Deca J, Poppe AR, Divin A, Lembège B (2021) The plasma environment surrounding the reiner gamma magnetic anomaly. J Geophys Res Space. https://doi.org/10.1029/2021JA029180

Dyal P, Parkin CW, Daily WD (1974) Magnetism and the interior of the moon. Rev Geophys 12(4):568–591. https://doi.org/10.1029/RG012i004p00568

Eastwood JP, Sibeck DG, Angelopoulos V, Phan TD, Bale SD, McFadden JP, Cully CM, Mende SB, Larson D, Frey S, Carlson CW, Glassmeier K-H, Auster HU, Roux A, Le CO (2008) THEMIS observations of a hot flow anomaly: solar wind, magnetosheath, and ground-based measurements. Geophys Res Lett 35:L17S03. https://doi.org/10.1029/2008GL033475

Fatemi S, Holmström M, Futaana Y, Barabash S, Lue C (2013) The lunar wake current systems. Geophys Res Lett 40:17–21. https://doi.org/10.1029/2012GL054635

Futaana Y, Machida S, Saito Y, Matsuoka A, Hayakawa H (2001) Counterstreaming electrons in the near vicinity of the moon observed by plasma instruments on board NOZOMI. J Geophys Res 106:18729–18740. https://doi.org/10.1029/2000JA000146

Halekas JS, Brain DA, Mitchell DL, Lin RP, Harrison L (2006a) On the occurrence of magnetic enhancements caused by solar wind interaction with lunar crustal fields. Geophys Res Lett 33:L08106. https://doi.org/10.1029/2006GL025931

Halekas JS, Brain DA, Mitchell DL, Lin RP (2006b) Whistler waves observed near lunar crustal magnetic sources. Geophys Res Lett 33:L22104. https://doi.org/10.1029/2006GL027684

Halekas JS, Poppe AR, McFadden JP, Angelopoulos V, Glassmeier K-H, Brain DA (2014) Evidence for small-scale collisionless shocks at the moon from ARTEMIS. Geophys Res Lett 41:7436–7443. https://doi.org/10.1002/2014GL061973

Halekas JS, Poppe AR, Lue C, Farrell WM, McFadden JP (2017) Distribution and solar wind control of compressional solar wind-magnetic anomaly interactions observed at the moon by ARTEMIS. J Geophys Res Space Phys 122:6240–6254. https://doi.org/10.1002/2017JA023931

Harada Y, Halekas JS (2016) Upstream waves and particles at the moon. In: Keiling A, Lee D-H, Nakariakov V (eds) Low-frequency waves in space. John Wiley Sons Inc, Hoboken NJ

Harada Y, Halekas JS, Poppe AR, Tsugawa Y, Kurita S, McFadden JP (2015) Statistical characterization of the foremoon particle and wave morphology: ARTEMIS observations. J Geophys Res Space Phys 120:4907–4921. https://doi.org/10.1002/2015JA021211

Holmström M, Fatemi S, Futaana Y, Nilsson H (2012) The interaction between the moon and the solar wind. Earth Planet Space 64:17. https://doi.org/10.5047/eps.2011.06.040

Hood LL, Zakharian A, Halekas J, Mitchell DL, Lin RP, Acuña MH, Binder AB (2001) Initial mapping and interpretation of lunar crustal magnetic anomalies using lunar prospector magnetometer data. J Geophys Res 106(E11):27825–27839. https://doi.org/10.1029/2000JE001366

Kato M, Sasaki S, Takizawa Y (2010) The Kaguya mission overview, *Space Sci. Rev* 154:3–19. https://doi.org/10.1007/s11214-010-9678-3

Nakagawa *et al. Earth, Planets and Space*   (2023) 75:60

Page 14 of 14

Lin RP, Mitchell DL, Curtis DW, Anderson KA, Carlson CW, McFadden J, Acuna MH, Hood LL, Binder A (1998) Lunar surface magnetic fields and their interaction with the solar wind: results from lunar prospector. Science 281(5382):1480–1484. https://doi.org/10.1126/science.281.5382.1480

LRO Project and Lunar Geodesy and Cartography Working Group (2008), A standardized lunar coordinate system for the Lunar Reconnaissance Orbiter and lunar datasets, LRO Project and LGCWG White Paper, version 5, Goddard Space Flight Center, National Aeronautics and Space Administration, http://lunar.gsfc.nasa.gov/library/LunCoordWhitePaper-10-08.pdf.

Lue C, Futaana Y, Barabash S, Wieser M, Holmström M, Bhardwaj A, Dhanya MB, Wurz P (2011) Strong influence of lunar crustal fields on the solar wind flow. Geophys Res Lett 38:L03202. https://doi.org/10.1029/2010GL046215

Lyon EF, Bridge HS, Binsak JH (1967) Explorer 35 plasma measurements in the vicinity of the moon. J Geophys Res 72:6113

McComas DJ, Allegrini F, Bochsler P, Frisch P, Funsten HO, Gruntman M, Janzen PH, Kucharek H, Möbius E, Reisenfeld DB, Schwadron NA (2009) Lunar backscatter and neutralization of the solar wind: first observations of neutral atoms from the moon. Geophys Res Lett. https://doi.org/10.1029/2009GL038794

Mitchell DL, Halekas JS, Lin RP, Frey S, Hood LL, Acuña MH, Binder A (2008) Global mapping of lunar crustal magnetic fields by lunar prospector. Icarus 194:401–409. https://doi.org/10.1016/j.icarus.2007.10.027

Nakagawa T (2016) ULF/ELF waves in the near-moon space. John Wiley, Hoboken, NJ. https://doi.org/10.1002/9781119055006

Nakagawa T, Takahashi F, Tsunakawa H, Shibuya H, Shimizu H, Matsushima M (2011) Non-monochromatic whistler waves detected by Kaguya on the dayside surface of the moon. Earth Planets Space 63(1):37–46. https://doi.org/10.5047/eps.2010.01.005

Nakagawa T, Nakayama A, Takahashi F, Tsunakawa H, Shibuya H, Shimizu H, Matsushima M (2012) Large-amplitude monochromatic ULF waves detected by Kaguya at the moon. J Geophys Res 117:A04101. https://doi.org/10.1029/2011JA017249

Ness NF, Behannon KW, Taylor HE, Whang YC (1968) Perturbations of the interplanetary magnetic field by the lunar wake. J Geophys Res 73:3421–3440

Neugebauer M, Clay DR, Goldstein BE, Tsurutani BT, Zwickl RD (1984) A reexamination of rotational and tangential discontinuities in the solar wind. J Geophys Res 89(A7):5395–5408. https://doi.org/10.1029/JA089iA07p05395

Ogilvie KW, Steinberg JT, Fitzenreiter RT, Owen CJ, Lazarus AJ, Farrell WM, Torbert RB (1996) Observation of the lunar plasma wake from the WIND spacecraft on December 27, 1994. Geophys Res Lett 23:1255–1258

Owen CJ, Lepping RP, Ogilvie KW, Slavin JA, Farrell WM, Byrnes JB (1996) The lunar wake at 68 RL: WIND magnetic field observations. Geophys Res Lett 23:1263–1266

Poppe AR, Sarantos M, Halekas JS, Delory GT, Saito Y, Nishino M (2014) Anisotropic solar wind sputtering of the lunar surface induced by crustal magnetic anomalies. Geophys Res Lett 41:4865–4872. https://doi.org/10.1002/2014GL060523

Poppe AR, Halekas JS, Lue C, Fatemi S (2017) ARTEMIS observations of the solar wind proton scattering function from lunar crustal magnetic anomalies. J Geophys Res Planets 122:771–783. https://doi.org/10.1002/2017JE005313

Russell CT, Lichtenstein BR (1975) On the source of lunar limb compressions. J Geophys Res 80(34):4700–4711. https://doi.org/10.1029/JA080i034p04700

Saito Y, Yokota S, Tanaka T, Asamura K, Nishino MN, Fujimoto M, Tsunakawa H, Shibuya H, Matsushima M, Shimizu H, Takahashi F, Mukai T, Terasawa T (2008) Solar wind proton reflection at the lunar surface: low energy ion measurement by MAP-PACE onboard SELENE (KAGUYA). Geophys Res Lett 35:24205. https://doi.org/10.1029/2008GL036077

Saito Y, Yokota S, Asamura K, Tanaka T, Nishino MN, Yamamoto T, Terakawa Y, Fujimoto M, Hasegawa H, Hayakawa H, Hirahara M, Hoshino M, Machida S, Mukai T, Nagai T, Nagatsuma T, Nakagawa T, Nakamura M, Oyama K-i, Sagawa E, Sasaki S, Seki K, Shinohara I, Terasawa T, Tsunakawa H, Shibuya H, Matsushima M, Shimizu H, Takahashi F (2010) In-flight performance and initial results of plasma energy angle and composition experiment (PACE) on SELENE (Kaguya). Space Sci Rev 154:265–303. https://doi.org/10.1007/s11214-010-9647-x

Saito Y, Nishino MN, Fujimoto M, Yamamoto T, Yokota S, Tsunakawa H, Shibuya H, Matsushima M, Shimizu H, Takahashi F (2012) Simultaneous observation of the electron acceleration and ion deceleration over lunar

magnetic anomalies. Earth Planets Space 64:83–92. https://doi.org/10.5047/eps.2011.07.011

Schubert G, Lichtenstein BR (1974) Observations of moon-plasma interactions by orbital and surface experiments. Rev Geophys Space Phys 12:592–626

Schwartz SJ (1995) Hot flow anomalies ear the Earth's bow shock. Adv Space Res 15(8/9):107–116

Schwartz SJ, Paschmann G, Sckopke N, Bauer TM, Dunlop MW, Fazakerley AN, Thomsen MF (2000) Conditions for the formation of hot flow anomalies at the earth's bow shock. J Geophys Res 105:12639–12650

Shimizu H, Takahashi F, Horii N, Matsuoka A, Matsushima M, Shibuya H, Tsunakawa H (2008) Ground calibration of the high-sensitivity SELENE lunar magnetometer LMAG. Earth Planets Space 60:353–363. https://doi.org/10.1186/BF03352800

Sonett CP (1982) Electromagnetic induction in the Moon. Rev Geophys 20(3):411–455. https://doi.org/10.1029/RG020i003p00411

Sonnerup BU, Cahill LJ (1967) Magnetopause structure and attitude from Explorer 12 observations. J Geophys Res 72(1):171–183. https://doi.org/10.1029/JZ072i001p00171

Takahashi F, Shimizu H, Matsushima M, Shibuya H, Matsuoka A, Nakazawa S, Iijima Y, Otake H, Tsunakawa H (2009) In-orbit calibration of the lunar magnetometer onboard SELENE (KAGUYA). Earth Planets Space 61:1269–1274. https://doi.org/10.1186/BF03352979

Thomas VA, Winske D, Thomsen MF, Onsager TG (1991) Hybrid simulation of the formation of a hot flow anomaly. J Geophys Res 96(A7):11625–11632. https://doi.org/10.1029/91JA01092

Tsugawa Y, Terada N, Katoh Y, Ono T, Tsunakawa H, Takahashi F et al (2011) Statistical analysis of monochromatic whistler waves near the moon detected by Kaguya. Ann Geophys 29:889–893. https://doi.org/10.5194/angeo-29-889-2011

Tsugawa Y, Katoh Y, Terada N, Ono T, Tsunakawa H, Takahashi F, Shibuya H, Shimizu H, Matsushima M, Saito Y, Yokota S, Nishino MN (2012) Statistical study of broadband whistler-mode waves detected by Kaguya near the moon. Geophys Res Lett 39:L16101. https://doi.org/10.1029/2012GL052818

Tsunakawa H, Shibuya H, Takahashi F, Shimizu H, Matsushima M, Matsuoka A, Nakazawa S, Otake H, Iijima Y (2010) Lunar magnetic field observation and initial global mapping of lunar magnetic anomalies by MAP-LMAG onboard SELENE (Kaguya). Space Sci Rev 154:219–251. https://doi.org/10.1007/s11214-010-9652-0

Tsunakawa H, Takahashi F, Shimizu H, Shibuya H, Matsushima M (2015) Surface vector mapping of magnetic anomalies over the moon using Kaguya and lunar prospector observations. J Geophys Res Planets 120:1160–1185. https://doi.org/10.1002/2014JE004785

Wang X-D, Bian W, Wang J-S, Liu J-J, Zou Y-L, Zhang H-B, Lü C, Liu J-Z, Zuo W, Su Y, Wen W-B, Wang M, Ouyang Z-Y, Li C-L (2010) Acceleration of scattered solar wind protons at the polar terminator of the moon: results from Chang'E-1/SWIDs. Geophys Res Lett 37:L07203. https://doi.org/10.1029/2010GL042891

Wieser M, Barabash S, Futaana Y, Holmström M, Bhardwaj A, Sridharan R, Dhanya MB, Wurz P, Schaufelberger A, Asamura K (2009) Extremely high reflection of solar wind protons as neutral hydrogen atoms from regolith in space. Planet Space Sci 57:2132–2134. https://doi.org/10.1016/j.pss.2009.09.012

Wieser M, Barabash S, Futaana Y, Holmström M, Bhardwaj A, Sridharan R, Dhanya MB, Wurz P, Schaufelberger A, Asamura K (2011) Erratum to "Extremely high reflection of solar wind protons as neutral hydrogen atoms from regolith in space." Planet Space Sci 57:798–799. https://doi.org/10.1016/j.pss.2011.01.016

Zimmerman MI, Farrell WM, Poppe AR (2015) Kinetic simulations of kilometer-scale mini-magnetosphere formation on the Moon. J Geophys Res Planets 120:1893–1903. https://doi.org/10.1002/2015JE004865

Publisher's Note